ELMER PRESS

Original Article

World J Oncol. 2024;15(1):114-125

Establishment and Characterization of a New Intrahepatic Cholangiocarcinoma Cell Line, ICC-X2

Hao Xu[a, b, h], Chang Peng Chai[a, c, h], Huan Tang[c, h], Yuan Hui Su[c], Cheng Yu[c, d], Lu Li[a], Jian Feng Yi[b, e], Zhen Zhen Ye[c], Zheng Feng Wang[a, c], Jin Jing Hu[a], Wei Luo[a], Hui Zhang[c, f], Xin Miao[g, i], Wen Ce Zhou[c, f, i]

Abstract

Background: Intrahepatic cholangiocarcinoma (ICC) is an aggressive malignant tumor of the biliary tract that is prone to recurrence and metastasis and is characterized by poor sensitivity to chemotherapy and overall prognosis. For these reasons, there is an urgent need to understand its pathological mechanisms and develop effective treatments. To address this challenge, the establishment of suitable preclinical models is critical.

Methods: Fresh ICC tissue samples were used for primary culture and subculture. The cell line was evaluated by cell proliferation assays, clonal formation assays, karyotype analysis, and short tandem repeat (STR) analysis. Drug resistances against oxaliplatin, paclitaxel, gemcitabine and 5-fluorouracil (5-FU) were evaluated by CCK-8 assay. Subcutaneous injection of 1×10^6 cells to three BALB/c nude mice was conducted for xenograft studies. The hematoxylin and eosin (H&E) staining was used to detect the pathological status of the cell line. The expression of biomarkers CK7, CK19, Ki-67, E-cadherin and vimentin was determined by immunocytochemistry assay.

Results: A new ICC cell line named ICC-X2 was successfully established. Like ICC-X3 established using the same patient's metastatic tumor, the cell line has been continuously cultured *in vitro* for more than a year and has been passaged more than 100 times. ICC-X2 retained the typical biliary epithelial morphology. The population doubling time of ICC-X2 is 48 h. The cells demonstrated an abnormal nearly tetraploid karyotype. The STR analysis confirmed that ICC-X2 was highly consistent with the primary tumor tissue and not cross-contaminated by existing cell lines. ICC-X2 cells positively expressed CK7, CK19, E-cadherin, and vimentin, and the positive expression of Ki-67 in ICC-X2 cells was 40%. The ICC-X2 cells exhibited a strong clonogenic ability. The drug sensitivity test indicated that ICC-X2 was sensitive to oxaliplatin and paclitaxel, but naturally resistant to gemcitabine and 5-FU. ICC-X2 was rapidly able to form transplanted tumors *in vivo* after subcutaneous inoculation in nude mice.

Conclusions: ICC-X2 is an excellent experimental model that can be used for studying the occurrence, development, and metastasis of ICC and investigating the mechanism of tumor drug resistance.

Keywords: Intrahepatic cholangiocarcinoma; Cell line; Establishment; Xenograft; Animal model

Manuscript submitted November 4, 2023, accepted December 11, 2023
Published online January 10, 2024

[a]The Fourth Department of General Surgery, the First Hospital of Lanzhou University, Lanzhou 730000, China
[b]The First Clinical Medical College, Lanzhou University, Lanzhou 730000, China
[c]The Second Clinical Medical College, Lanzhou University, Lanzhou 730000, China
[d]Department of Anesthesiology, Lanzhou University Second Hospital, Lanzhou 730000, China
[e]Department of Surgery, The First School of Clinical Medicine of Gansu University of Chinese Medicine, Lanzhou 730000, China
[f]Department of General Surgery, Lanzhou University Second Hospital, Lanzhou 730000, China
[g]State Key Laboratory of Veterinary Etiological Biology, Key Laboratory of Animal Virology of the Ministry of Agriculture, Lanzhou Veterinary Research Institute, Chinese Academy of Agricultural Sciences, Lanzhou 730000, China
[h]These authors contributed equally to this work.
[i]Corresponding Author: Xin Miao, State Key Laboratory of Veterinary Etiological Biology, Key Laboratory of Animal Virology of the Ministry of Agriculture, Lanzhou Veterinary Research Institute, Chinese Academy of Agricultural Sciences, Lanzhou 730000, China. Email: summermiaox@126.com; Wen Ce Zhou, Department of General Surgery, Lanzhou University Second Hospital, Lanzhou 730000, China. Email: zhouwc129@163.com

doi: https://doi.org/10.14740/wjon1757

Introduction

Intrahepatic cholangiocarcinoma (ICC) is the second most common primary malignant liver tumor, with a rising global incidence rate [1, 2]. Most ICC patients are in the advanced stage of the disease, and only 23-53.0% of them have the opportunity to undergo surgery [3-5]. However, due to postoperative recurrence and disease progression, the 5-year survival rate of patients after surgery is only 20-30% [6-8].

The prognostic factors of ICC include tumor size, multifocality, microvascular invasion (MVI), nerve invasion, and lymph node metastasis [9-12]. Studies have indicated that even in the early stages of ICC without MVI and lymph node metastasis, the recurrence rate in patients after resection may still be as high as 60-80% [13-18]. Animal models are es-

sential transitional tools between cell lines and human clinical trials, and strong tools for studying carcinogenesis and tumor progression as well as testing the efficacy and toxicity of therapeutic compounds. When compared with the *in vitro* model, the animal model can better simulate the interactions between tumor and tumor microenvironment (TME), support the immune and vascular functions, and elucidate the mechanism of tumor cells, which cannot be replaced by the *in vitro* model [19].

In this study, a novel stable ICC cell line named ICC-X2 was established. It is an excellent experimental model that can be used for studying the occurrence, development, and metastasis of ICC and investigating the mechanism of tumor drug resistance.

Materials and Methods

Tissue source

The tissue sample was collected from the tumor tissue of a patient with ICC who had undergone surgical treatment in the First Hospital of Lanzhou University on July 23, 2021. This patient was a 62-year-old female with a liver tumor and had no history of smoking, drinking, and hepatitis B and hepatitis C infections. The level of alpha-fetoprotein (AFP) in the patient was 7.8 IU/mL (reference range: 0 - 5.8 IU/mL), and the level of carcinoembryonic antigen (CEA) and carbohydrate antigen 19-9 (CA19-9) in the patient were within the normal range. The patient did not receive any preoperative treatment. The clinical data are shown in Table 1. Magnetic resonance imaging (MRI) showed that the tumor was in segment S4 of the liver, and had a size of 9 × 7 cm (Fig. 1a). The gross picture generally showed a huge tumor in segment S4 of the liver, with yellow and white sections and multiple satellite lesions around the tumor (Fig. 1b). The primary cells were extracted from the primary lesion and then subcultured.

The study was conducted according to the guidelines of the Declaration of Helsinki, and approved by the Ethics Committee of the First Hospital of Lanzhou University (LDYYLL2022-345).

The methods followed in this study, as described below, are similar or identical to those employed in previous studies [20-22].

Establishment of the cell lines

The tumor tissue sample was cleaned 3 - 5 times with sterile phosphate-buffered saline (PBS) (GIBCO) and then cut into small pieces of about 1 mm^3 with a sterile blade. The sample was placed in a mixed solution of type II collagenase (GIBCO) and dispase (Invitrogen) and then digested in a shaker at 37 °C. When the tissue block was half-digested, the supernatant was absorbed. After filtration with a 100-mesh filter screen, the supernatant was centrifuged at 300 × g for 3 min. Then, the supernatant was discarded, and the recovered cells were resuspended in PBS and centrifuged again at 300 × g for

Table 1. Clinical Data of the Patient Included in the Study

Cell line	Patient age/ethnicity	Gender	Current status (days)	Histopathology/differentiation	Tumor size (cm)	Prior therapy	Culture date	Microvascular invasion	Nerve invasion	Lymph node and distant metastasis	AJCC cancer staging	Serum		
												AFP (0 - 5.8 IU/mL)	CEA (0 - 5.2 ng/mL)	CA19-9 (0 - 35 U/mL)
ICC-X2	62/Asian	Female	NA	Moderately-poorly, some undifferentiated	9 × 7	None	July 23, 2021	No	Yes	Nos. 12 lymph nodes (2/2) and Nos. 13 lymph nodes (5/5); abdominal wall metastasis and omental metastasis	T2N1M0	7.8	1.7	24.9

AJCC: American Joint Committee on Cancer; AFP: alpha-fetoprotein; CEA: carcinoembryonic antigen; CA19-9: carbohydrate antigen 19-9.

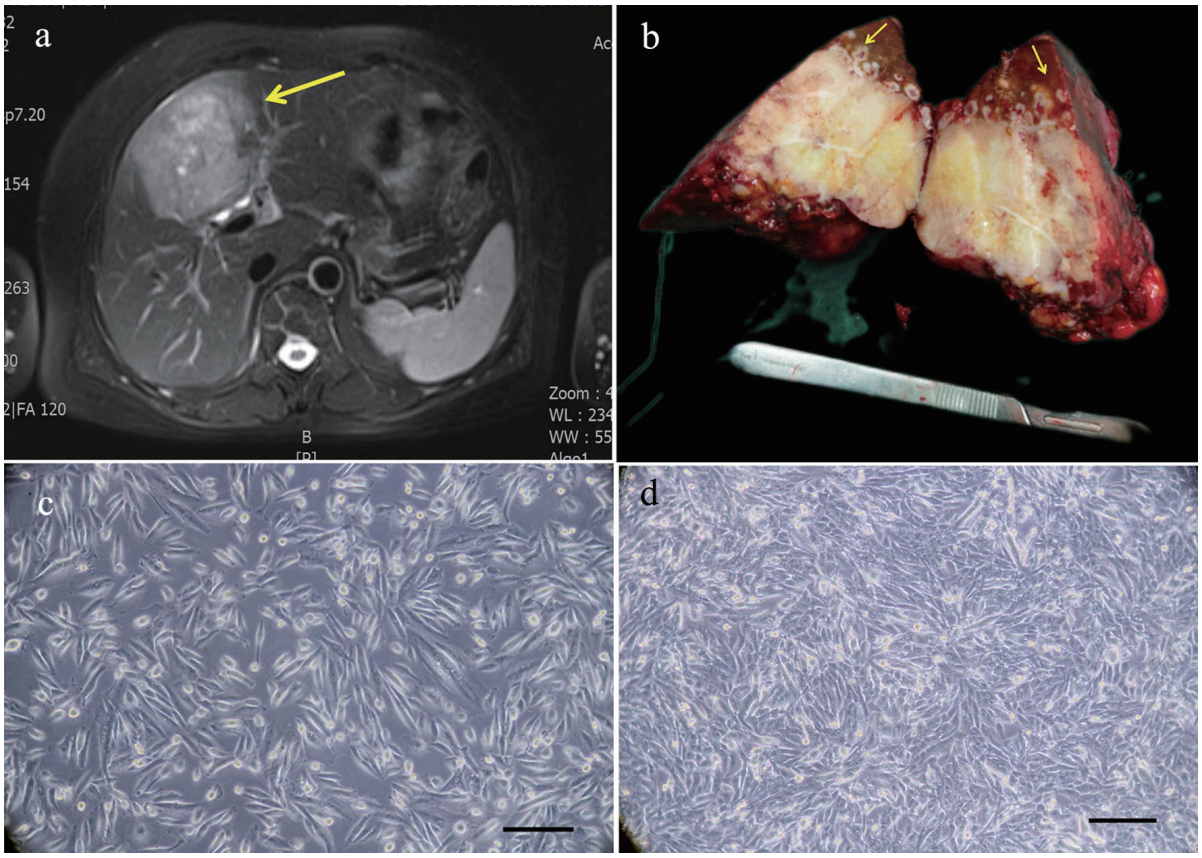

Figure 1. Relevant clinical data and morphology of the ICC-X2 cells. (a) MRI scan showing a large 9 × 7 cm lesion in segment IV of the liver (long arrow). (b) Gross view of the surgically resected specimen. Multiple satellite lesions can be observed around the primary lesion (short arrows). (c) Light microscope image of the ICC-X2 cells of passage 10. (d) Light microscope images of the ICC-X2 cells of passage 50 (scale bar = 100 µm). MRI: magnetic resonance imaging.

3 min. The final precipitate obtained was mixed with a complete culture medium (RPMI-1640 + 10% fetal bovine serum (FBS) + 1% penicillin and streptomycin, BI), and uniformly inoculated on a six-well plate (NEST). During the primary culture, the fibroblasts were mechanically scraped repeatedly with a 1 mL pipette gun under the microscope. After about 2 weeks, when the cells completely occupied the bottom of the culture plate, the culture solution in the plate was removed, and the plate was rinsed twice with PBS. The adherent cells on the surface of the culture plates were then digested with 0.25% trypsin for the passage of cell culture. The cell growth was regularly observed under a light microscope. From the fourth generation onwards, the cells were subcultured in a ratio of 1:2 and frozen with a reagent procured from Mei5 Biotechnology.

Cell growth curve

The 25th-generation cells in the logarithmic growth phase were collected after trypsin digestion and the cell density was adjusted to 1×10^4/mL. After mixing, 0.1 mL of inoculum was added to each well of a 96-well plate. Each sample was added to five wells. CCK-8 (Dojindo) reagent was added at the same time for 4 consecutive days after inoculation and allowed to react for 2 h. The UV absorbance value at 450 nm was measured using a microplate reader. The cell doubling time was calculated using the formula Td = t × Lg2/lg (N1/N0).

Analysis of short tandem repeats (STRs)

The 10th-generation cells in the logarithmic growth phase were collected after trypsin digestion, and the STR analysis was conducted by Suzhou Genetic Testing Biotechnology Company to determine the cross-contamination among cultured cells.

Karyotype analysis

The 40th-generation cells in the logarithmic growth phase were collected and treated with 0.25 µg/mL colchicine for 6 h at 37 °C overnight. The metaphase cells were then harvested and fixed with methanol glacial acetic acid (3:1). After trypsin digestion, the specimens were stained with Giemsa stain and counted under a microscope. The cells showing good disper-

sion and moderate staining during the metaphase stage of mitosis were selected for karyotype analysis.

Tumor sphere culture

The 30th-generation ICC-X2 cells in the logarithmic growth phase were digested followed by centrifugation. The cell concentrate was then washed twice with PBS, resuspended in the stem cell culture medium (RPMI-1640 + 1 × B27 + 20 ng/mL basic fibroblast growth factor (bFGF) + 20 ng/mL epidermal growth factor (EGF)), and then counted. The cells were cultivated in an ultra-low attachment six-well plate (Corning). A total of 1,000 cells were added to each well of the plate, and then 2 mL of culture medium was added for 14 days. The plate was observed under a microscope to determine the tumor sphere formation and the number of tumor spheres.

Organoid culture

Initially, the matrigel (Corning) was dissolved at 4 °C, and the 24-well plate and centrifuge tube were precooled at -20 °C. The 30th-generation ICC-X2 cells in the logarithmic growth phase were digested, resuspended, and counted. A total of 1×10^4 cells along with 30 µL matrix glue and 30 µL complete medium were added to each cell of the plate. The addition was carried out on an ice bath, and care was taken to avoid bubbles during the whole process. The 24-well plates were incubated in an incubator at 37 °C for 30 min. After full solidification, 500 µL of complete medium was added to each well to cover the liquid drop and placed in an incubator at 37 °C for cell cultivation. The liquid in the plates was replaced every 2 days. The morphological changes in organoids were observed under a microscope.

Drugs

Gemcitabine was procured from Jiangsu Haosen Pharmaceutical Group Co., Ltd., oxaliplatin was procured from Jiangsu Hengrui Pharmaceutical Co., Ltd., 5-FU was procured from Tianjin Jinyao Pharmaceutical Co., Ltd., and paclitaxel was procured from Jiangsu Aosaikang Pharmaceutical Co., Ltd.

Drug sensitivity test

The 45th-generation ICC-X2 cells in the logarithmic growth phase were digested with trypsin and collected to prepare a single-cell suspension. Each well of a 96-well plate was inoculated with 10,000 cells/100 µL, with each test repeated in six wells. After the cells adhered to the wall, different concentrations of anti-tumor drugs were added to the experimental group. Equal volumes of solvent of each drug group were added to the vehicle control group. After 72 h of drug action, the complete medium was replaced by 8 µL of 100% serum-free medium containing 10% (v/v) CCK. Then, the optical density (OD) value was measured after 2 h at 450 nm.

BALB/c nude mice

The experimental animals used in this study were BALB/c nude female mice, 4 - 6 weeks old, weighing 16 to 20 g. The animals were purchased from Changzhou Kavens Experimental Animal Co., Ltd. and raised in the SPF Laboratory of the Animal Experiment Center of Lanzhou University. All the animal experiments have been reviewed and approved by the Medical Animal Experiment Ethics Committee of the First Hospital of Lanzhou University (LDYYLL2022-345).

Xenograft experiment

The 45th-generation cells in the logarithmic growth phase were collected after trypsin digestion, and the cell density was adjusted to 1×10^7/mL. Then, three BALB/c nude mice were inoculated with 0.1 mL of culture each into the middle and posterior parts of the left armpit for the construction of ICC-X2 nude mice xenograft. The tumor growth of the nude mice was observed and recorded every other day, and the tumor-bearing mice were killed 4 weeks later. The tumor tissue was then excised and fixed with 10% formalin. Further, routine histopathological and immunohistochemical (IHC) examinations were performed on the harvested tissues.

Hematoxylin and eosin (H&E) and IHC staining

The 40th-generation cells were digested and inoculated onto a sterile slide for monitoring growth. After 48 h, the slides were washed with PBS, fixed with 4% paraformaldehyde for 15 min, dried, and then treated with 0.5% Triton X-100 for 20 min. The paraffin sections of similar organs, transplanted tumors, and primary tumors were prepared and baked at 60 °C overnight. The dewaxing, gradient alcohol hydration and antigen repair processes were completed using Dako's Autostainer Link 48 instrument. The samples were incubated in 3% hydrogen peroxide solution at 37 °C for 15 min to block the activity of peroxidase. The sections were blocked with drip diluted 100 µL normal goat serum and sealed at 37 °C for 15 min. The samples were incubated with Fuzhou Maxin ready-to-use antibodies (CK7, CK19, Ki-67, E-cadherin, and vimentin) at 37 °C for 1 h. DAB dye kit (Dako) was used for color development (the samples were washed under running water for 5 min for the removal of excess DAB). Dehydration and xylene transparency were carried out after hematoxylin counterstaining, and the sections were observed under a microscope after neutral resin sealing.

Statistical analysis

All the statistical analyses were performed using the SPSS 26.0 software. The data were expressed as mean ± standard deviation (SD). Student's *t*-tests and analysis of variance (ANOVA)

were applied for group comparisons. A P-value < 0.05 was considered statistically significant.

Results

Establishment of the ICC-X2 cell line

The human ICC cell line, named ICC-X2, which can be maintained by a continuous passage, was established by first extracting the primary tumor, obtaining the primary culture using the enzyme digestion method, and the removal of fibroblasts by mechanical scraping method. At present, the cell line has been continuously passaged for more than 100 generations and deposited in the Chinese Typical Culture Collection Center (CCTCC No. 202259).

Under the inverted microscope, it was observed that the cells were grown in a monolayer culture and lost contact inhibition. The cells were mainly spindle-shaped, and a few were polygonal and round (Fig. 1c). The cells had evident nucleoli. The cells maintained vigorous metabolism with each passage. The cell morphology and growth rate were stable, even after 80 generations (Fig. 1d).

Cell growth curve

CCK-8 was used for measuring the absorbance values of cells at 450 nm for 4 consecutive days. The cell growth curve was plotted with the culture time as the abscissa and the absorbance value as the ordinate (Fig. 2a). According to the equation: Td = tlg2/lg (N1/N0), the doubling time of ICC-X2 was computed to be 48 h.

Analysis of STRs of genomic DNA

The DNA typing results supported that the two submitted samples were from the same individual with a likelihood ratio (LR) of 5.0731×10^{20}. The STR profiles suggested a high match between ICC-X2 cells and tumor tissue (Fig. 2b), indicating that ICC-X2 was from the tumor tissue.

Karyotype analysis

The chromosomes were counted and analyzed in 10 metaphase cells with good dispersion and moderate staining. The results indicated that all the ICC-X2 cells were sub-tetraploid, with large differences in chromosome number and morphology. The representative karyotype was 77,XXX der(1)der(7)der(8) del(9)q(21) (Fig. 2c).

Tumor sphere and organoid culture

As shown in Figure 2d, ICC-X2 cells grow in suspension and form a well-structured tumor sphere in the ultra-low attachment plate under a serum-free culture medium, indicating that ICC-X2 had some stem cell characteristics. When the ICC-X2 cell line was inoculated into the matrix, it can be observed that the organoid formed gradually increased from small granules to simple sphere- or cyst-like structures (Fig. 2e). This tissue culture took 7 to 14 days depending on the tumor characteristics.

Drug sensitivity test

Gemcitabine, paclitaxel, 5-FU, and oxaliplatin are the most commonly used chemotherapy drugs for bile duct malignant tumors. The sensitivity of ICC-X2 to these drugs was evaluated. The results indicated that ICC-X2 was sensitive to oxaliplatin (IC_{50} = 2.9 μmol/L) (Fig. 3a) and paclitaxel (IC_{50} = 7.3 ng/mL) (Fig. 3b), but naturally resistant to gemcitabine (IC_{50} > 60 μmol/L) (Fig. 3c) and fluorouracil (IC_{50} = 176.9 μmol/L) (Fig. 3d).

Xenograft experiment

When the ICC-X2 cell suspensions were subcutaneously inoculated into three BALB/c nude mice, they showed 100% tumorigenicity (Fig. 4a). The ICC-X2 xenograft tumor exhibited a spiky structure and a strong infiltration (Fig. 4b). The xenograft tumors developed rapidly, with the diameter of the tumor close to 1 cm at 4 weeks (Fig. 4c). No metastatic lesions were observed in other organs of the transplanted mice within 4 weeks (Fig. 4d). Figure 4e and f shows the tumor volume and weight curves of BALB/c nude mice, respectively.

H&E and IHC staining

H&E staining indicated that the ICC-X2 cells exhibited a spindle-shaped morphology, with enlarged nuclei, obvious nucleoli, and less cytoplasm (Fig. 5a). On the other hand, H&E staining of the organoids demonstrated that ICC-X2 formed gland-like structures. The cells in the organoids were closely connected, with lumen-like structures inside (Fig. 5b).

The postoperative pathological diagnosis of the primary tumor in the patient demonstrated moderately to poorly differentiated ICC (Fig. 5c1), some of which were undifferentiated carcinoma (Fig. 5c2).

H&E staining of the xenograft tumors demonstrated deep staining of the nuclei of the transplanted tumor cells in the ICC-X2 cell lines, obvious nucleoli and several mitotic figures. Different cell morphologies in xenograft tumors were observed. Some cells formed gland-like structures (Fig. 5d1), while some cells were spindle-shaped (Fig. 5d2) similar to fibroblasts. The histological morphology of the xenograft tumor was similar to that of the primary tumor. These indicated that the ICC-X2 cells retained good tumor heterogeneity as the primary tumor.

Further IHC detection of cell lines, organoids, xenografts, and the primary tumor demonstrated positive expression of CK7 (Fig. 6a1-d1) and CK19 (Fig. 6a2-d2), thereby confirm-

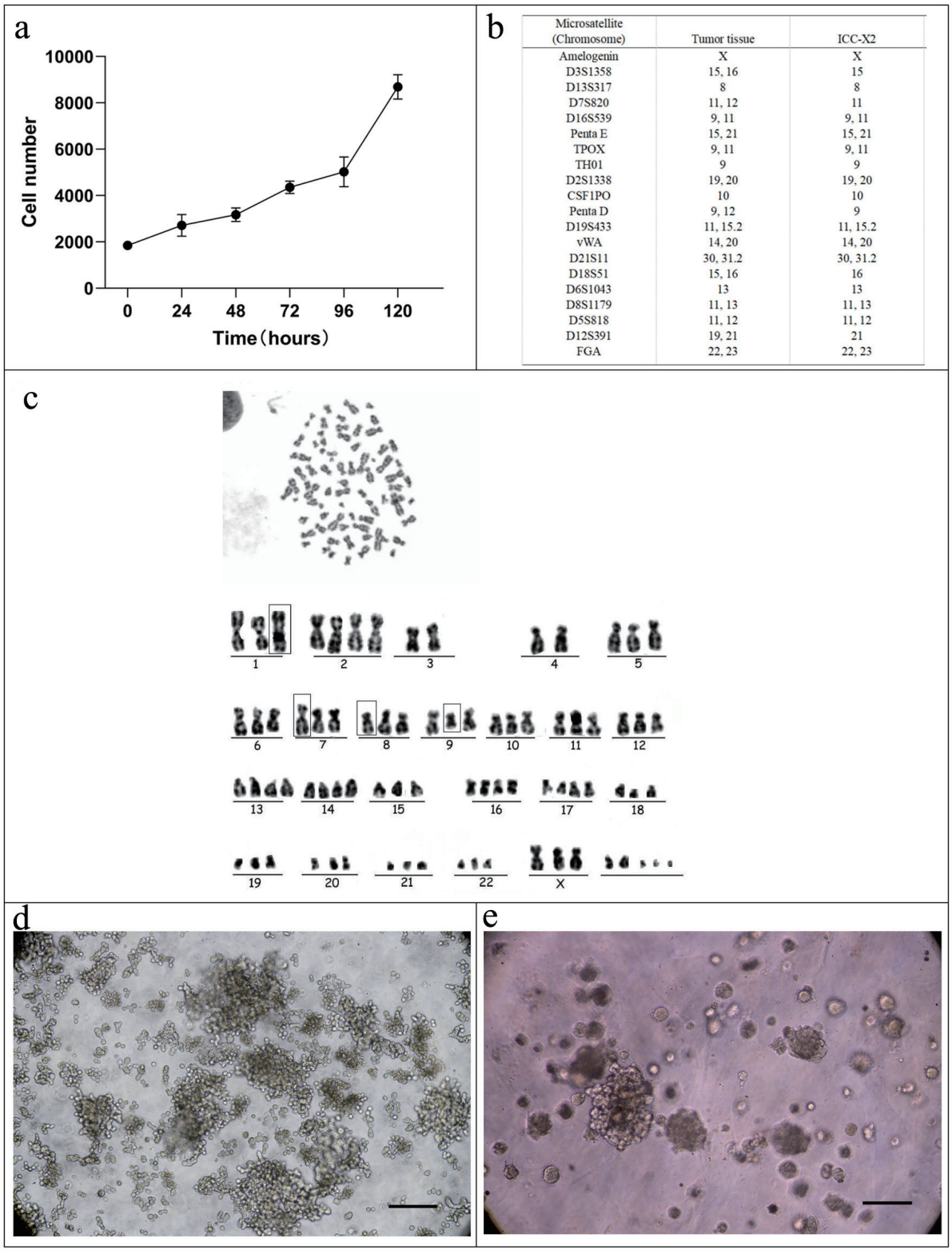

Microsatellite (Chromosome)	Tumor tissue	ICC-X2
Amelogenin	X	X
D3S1358	15, 16	15
D13S317	8	8
D7S820	11, 12	11
D16S539	9, 11	9, 11
Penta E	15, 21	15, 21
TPOX	9, 11	9, 11
TH01	9	9
D2S1338	19, 20	19, 20
CSF1PO	10	10
Penta D	9, 12	9
D19S433	11, 15.2	11, 15.2
vWA	14, 20	14, 20
D21S11	30, 31.2	30, 31.2
D18S51	15, 16	16
D6S1043	13	13
D8S1179	11, 13	11, 13
D5S818	11, 12	11, 12
D12S391	19, 21	21
FGA	22, 23	22, 23

Figure 2. Cell growth curve, karyotyping analysis, DNA STR analysis, tumor sphere, and organoid culture of the ICC-X2 cells. (a) Growth curve of the ICC-X2 cells. The doubling time of the ICC-X2 cells is 48 h. (b) Representative karyotype of the ICC-X2 cells. The cells exhibit hypotetraploid karyotypes with large differences in chromosome number and morphology. (c) STR analysis indicates that the ICC-X2 cells are highly consistent with the primary tumor tissue. (d) Two-week tumor sphere culture of ICC-X2. (e) Two-week ICC-X2 organoid culture (scale bar = 100 μm). STR: short tandem repeat.

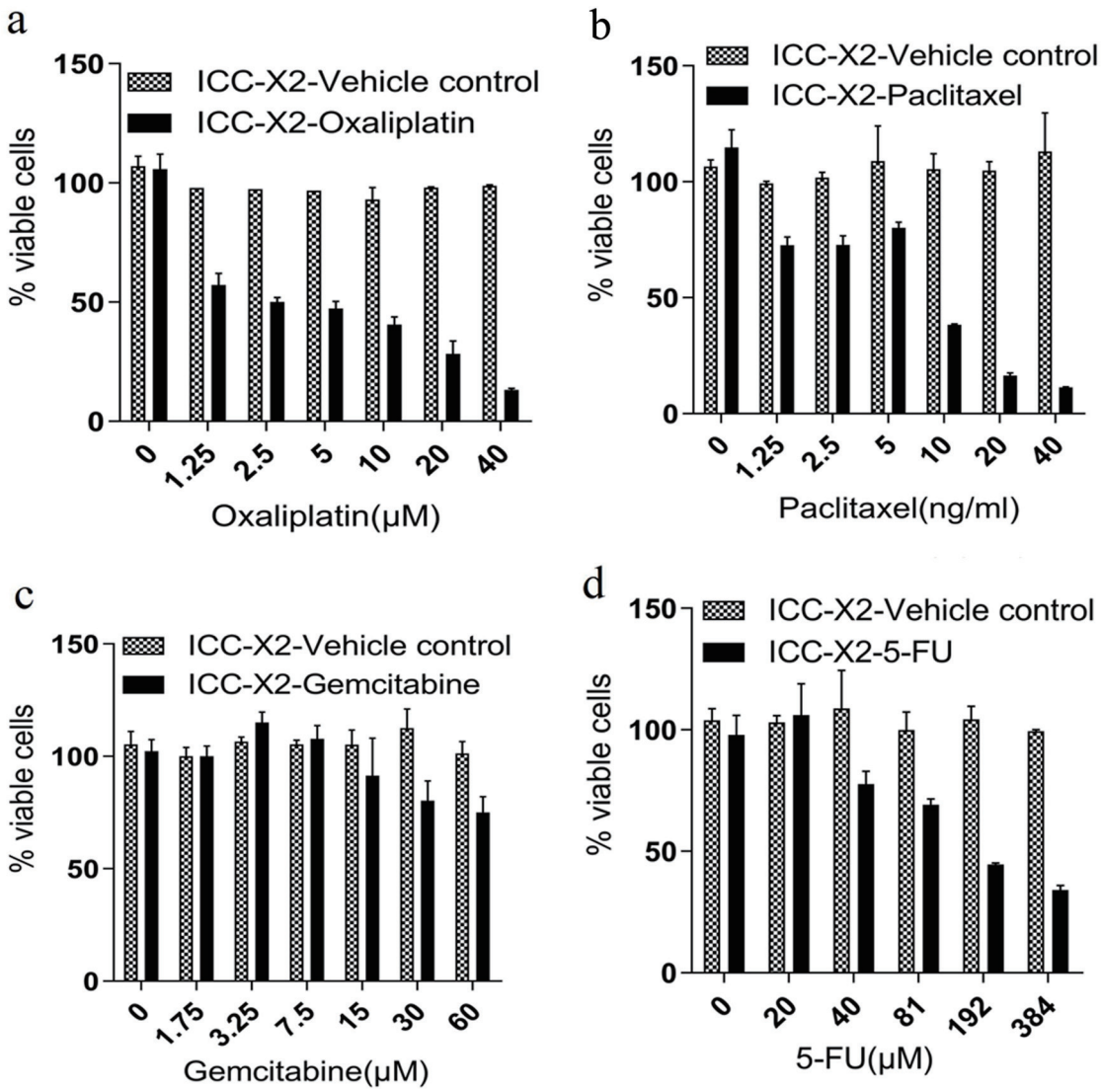

Figure 3. Drug sensitivity of the ICC-X2 cells. Dose-dependent effects of (a) paclitaxel, (b) gemcitabine, (c) oxaliplatin, and (d) 5-FU in the ICC-X2 cells. The cell line was sensitive to oxaliplatin and naturally resistant to gemcitabine, paclitaxel, and 5-FU. 5-FU: 5-fluorouracil.

ing that they originated from bile duct epithelium. Moreover, a high proportion for 40% of Ki-67 was expressed in all the cells, which was consistent with the rapid tumor proliferation and represents the malignant tumor characteristics (Fig. 6a3-d3). The simultaneous expression of E-cadherin (Fig. 6a4-d4) and vimentin (Fig. 6a5-d5) indicated that these cells have epithelial-mesenchymal transition (EMT) characteristics, which is also consistent with the clinical manifestations of multiple satellite lesions.

Discussion

ICC is a highly fatal disease with a poor prognosis. Postoperative recurrence and drug resistance are the major causes of death [16-18, 23, 24]. In this study, a new ICC cell line, i.e., ICC-X2 was established from the primary tumor of a Chinese female patient. Previously, we established an ICC cell line ICC-X3 using the patient's metastatic tumor [22].

At present, the cells have been continuously passaged for more than 100 generations. The doubling time of the cell population is 48 h, and the cell proliferation was vigorous. The STR analysis indicated that ICC-X2 and primary tumor tissues were highly consistent, proving that ICC-X2 is a new ICC cell line without cross-contamination. H&E staining of ICC-X2 demonstrated diverse cell morphology, mainly spindle-shaped, with an enlarged nucleus and darker staining. Moreover, the ratio of the nucleus to the cytoplasm was unbalanced, similar to that of HuH-28 cells. The IHC staining indicated that the ICC-X2 cells, organoids, xenograft, and primary tumor were all positive for both CK7 and CK19, which confirmed that they originated from the bile duct epithelium. In addition, the high

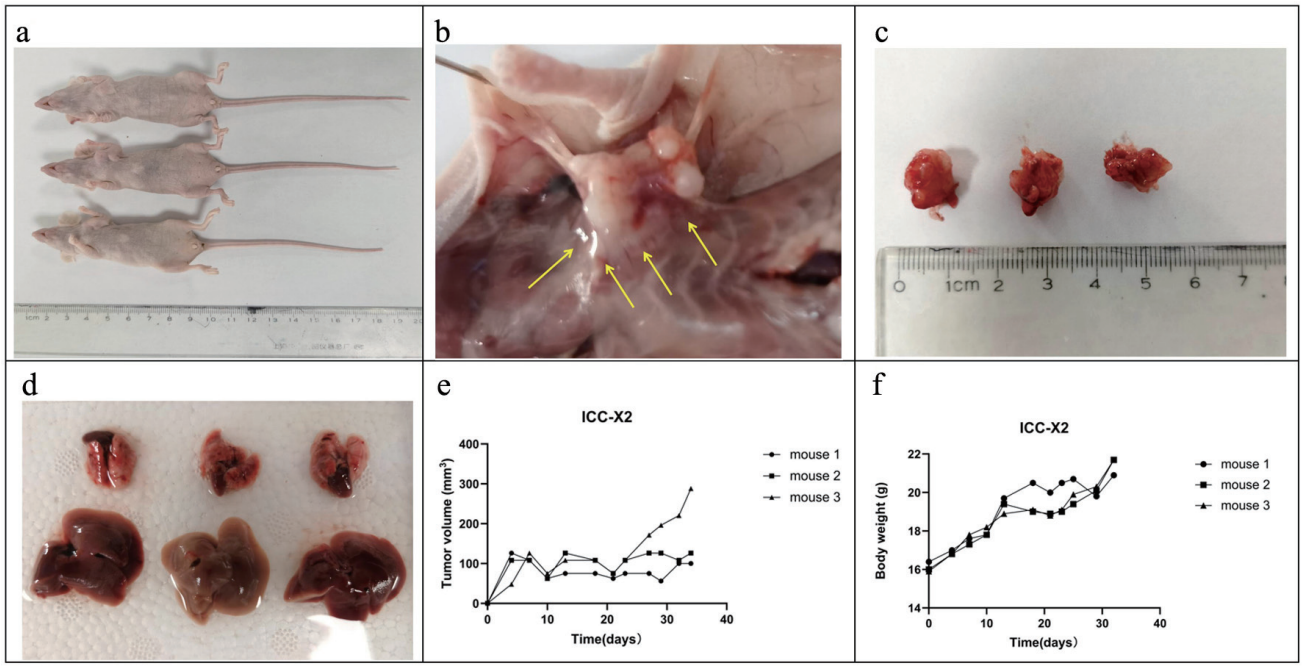

Figure 4. Tumorigenicity in BALB/C nude mice. (a) ICC-X2 cells can rapidly form xenografts after inoculation into BALB/C nude mice. (b) ICC-X2 xenograft tumors demonstrate stronger peritumoral infiltration (arrow). (c) Xenograft tumors develop rapidly, and the diameter of the tumor is close to 1 cm at 4 weeks. (d) No metastatic lesions are observed in other organs of the transplanted mice within 4 weeks. (e) Tumor volume curve when the ICC-X2 cells were inoculated into BALB/C nude mice. (f) Weight curve when the ICC-X2 cells were inoculated into BALB/C nude mice.

proportion of Ki-67 expression was consistent with the rapid proliferation of the tumor and represents the malignant tumor characteristics. The simultaneous expression of E-cadherin and vimentin indicated that the cells exhibited the characteristics of EMT and were consistent with the clinical manifestations of multiple satellite lesions.

Chemotherapy is the major treatment for postoperative and advanced ICC. As a result of the heterogeneity of drug-metabolizing enzymes and the heterogeneity of tumors in patients, every individual patient has a different sensitivity to different chemotherapy drugs, and even the congenital drug resistance is different [25, 26]. In this study, ICC-X2 was sensitive to oxaliplatin and paclitaxel, while it was naturally resistant to gemcitabine and 5-FU, which are commonly used clinical drugs. It is a good model for understanding the mechanism of drug resistance.

As an important step in tumor research, the mouse xenograft model is widely used in investigating the *in vivo* tumor biological behavior, preclinical detection of pharmacodynamics, and research and development of novel anti-tumor drugs [27]. However, several cell lines inoculated in nude mice cannot form xenografts, which greatly limits the research on tumor mechanisms. For example, HuH-28, RBE, HCCC-9810, and other ICC cell lines cannot form xenografts [28, 29]. The reason was considered to be related to the strong autoantigenicity or the strong residual innate immunity in mice [20, 30, 31]. After ICC-X2 was inoculated into the immune-deficient mice, the xenograft was rapidly formed. The characteristics of this model include a shorter incubation period, a simple inoculation process, and a 100% xenograft formation rate. Thus, it was a good *in vivo* model for research.

Conclusion

In conclusion, a new ICC cell line was established in this study. It is an excellent experimental model that can be used for investigating the mechanism of ICC invasion, metastasis, and drug resistance.

Acknowledgments

None to declare.

Financial Disclosure

This work was supported by grants from National Natural Science Foundation of China (grant 82260555), Natural Science Foundation of Gansu Province (grants 22JR11RA022, 23JRRA0929 and 23JRRA1601), Science and Innovation Foundation of Gansu University of Chinese Medicine (grants 2020KCZD-6 and 2020KCYB-10), Lanzhou Science and Technology Plan Project (grants 2022-3-45, 2020-ZD-60 and 2023-2-38), The Fund of The First Hospital of Lanzhou University (grant ldyyyn2022-12), Chengguan District Science and Technology Plan (grant 2023SHFZ0018).

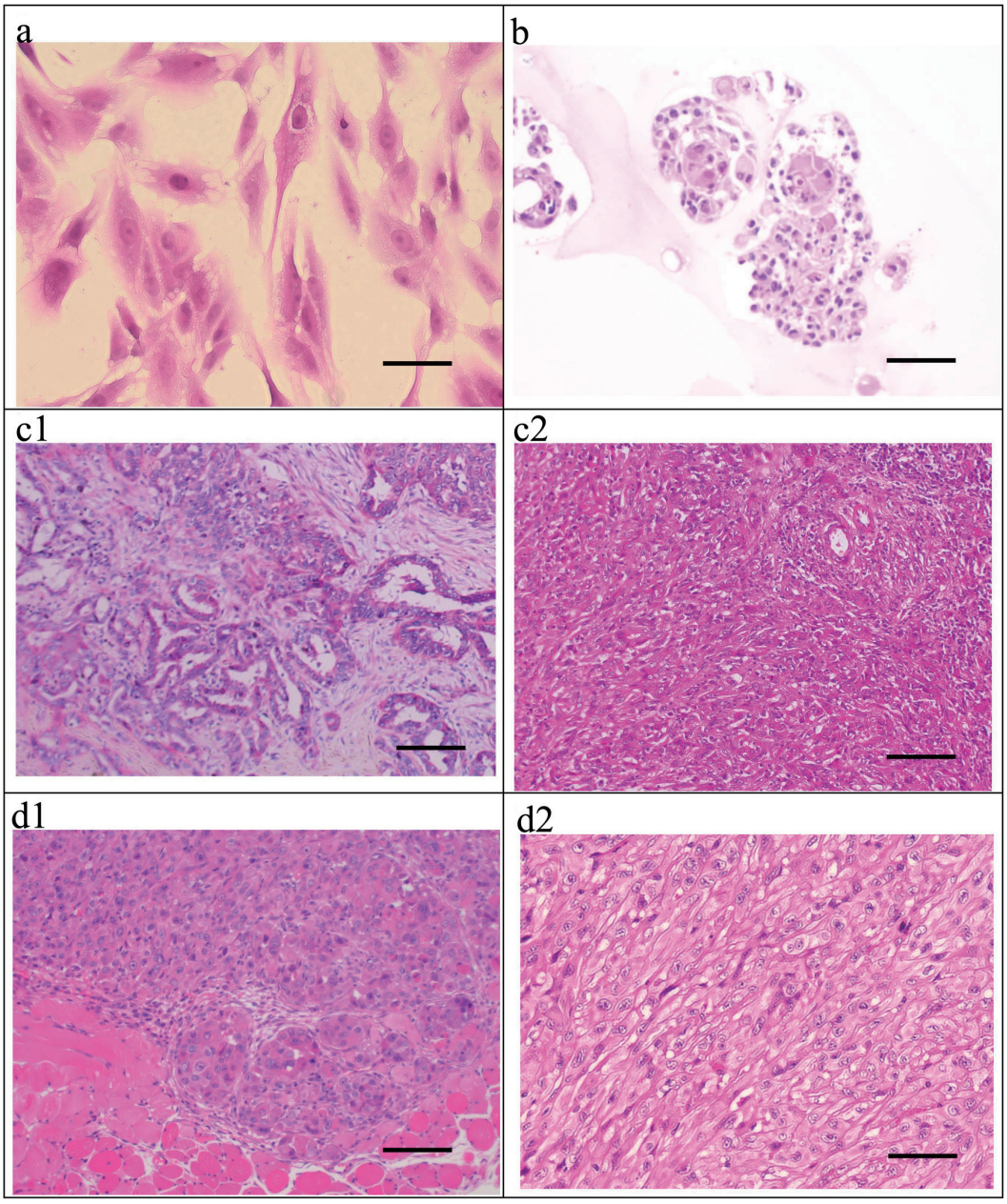

Figure 5. H&E staining of the ICC-X2 cells, organoids, primary tumor, and xenograft tumor. (a) H&E staining of the ICC-X2 cells. (b) H&E staining of the ICC-X2 organoids. H&E staining of the primary tumor shows moderately to poorly differentiated ICC, and the cancer cells are mainly polygonal and round (c1), some of which are undifferentiated cells, as indicated by their spindle-shaped appearance (c2). H&E staining of the xenograft tumors demonstrates that some cells form gland-like structures (d1), while some cells are spindle-shaped (d2) similar to fibroblasts (scale bar = 50 µm). H&E: hematoxylin and eosin.

Conflict of Interest

The authors declare no competing interests.

Informed Consent

We have obtained consents to publish this paper from all the participants of this study.

Author Contributions

XH, CCP, TH, SYH and YC performed identification of the cell line, and were major contributors in writing the manuscript. LL, YJF, YZZ and WZF analyzed and interpreted the results of the detection of this novel cell line, and wrote a part of the

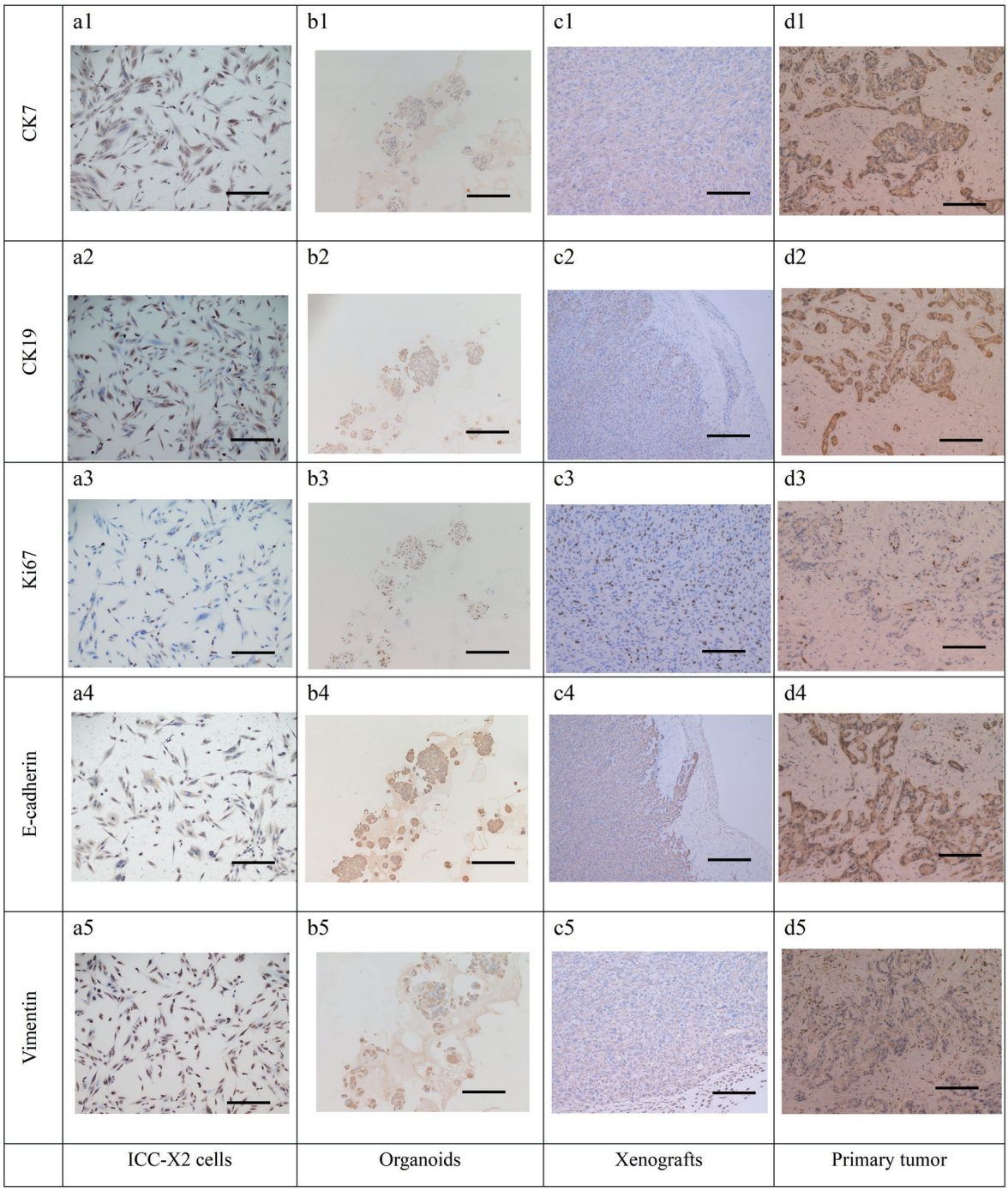

Figure 6. IHC staining of the cells, organoids, xenograft, and the primary tissue of ICC-X2. CK7 positive staining in cells (a1), organoids (b1), xenograft (c1), and the primary tissue (d1) of ICC-X2. CK19 positive staining in cells (a2), organoids (b2), xenograft (c2), and the primary tissue (d2) of ICC-X2. Ki-67 positive staining in cells (a3), organoids (b3), xenograft (c3), and the primary tissue (d3) of ICC-X2. E-cadherin positive staining in cells (a4), organoids (b4), xenograft (c4), and the primary tissue (d4) of ICC-X2. Vimentin positive staining in cells (a5), organoids (b5), xenograft (c5), and the primary tissue (d5) of ICC-X2 (scale bar = 100 µm). IHC: immunohistochemical.

manuscript. XH, CCP, TH, HJJ, LW and ZH were responsible for specimen collection. XH, CCP, TH, SYH, MX and ZWC modified the images and were involved in data processing. XH, CCP, TH and MX performed the cell culture. SYH, YC, LL, YJF, YZZ, WZF and HJJ produced the pathological sections. XH, CCP, TH, LW, ZH, MX and ZWC organized the data for all the experiments. XH, MX and ZWC conceived and designed and supervised the study. All authors reviewed the manuscript.

Data Availability

The data supporting the findings of this study are available from the corresponding author upon reasonable request.

References

1. Valle JW, Kelley RK, Nervi B, Oh DY, Zhu AX. Biliary tract cancer. Lancet. 2021;397(10272):428-444. doi pubmed
2. Kudo M, Izumi N, Kokudo N, Sakamoto M, Shiina S, Takayama T, Tateishi R, et al. Report of the 22nd nationwide follow-up Survey of Primary Liver Cancer in Japan (2012-2013). Hepatol Res. 2022;52(1):5-66. doi pubmed
3. Sakamoto Y, Kokudo N, Matsuyama Y, Sakamoto M, Izumi N, Kadoya M, Kaneko S, et al. Proposal of a new staging system for intrahepatic cholangiocarcinoma: Analysis of surgical patients from a nationwide survey of the Liver Cancer Study Group of Japan. Cancer. 2016;122(1):61-70. doi pubmed pmc
4. Dover LL, Jacob R, Wang TN, Richardson JH, Redden DT, Li P, DuBay DA. Improved postoperative survival for intraductal-growth subtype of intrahepatic cholangiocarcinoma. Am Surg. 2016;82(11):1133-1139. pubmed pmc
5. Fong ZV, Brownlee SA, Qadan M, Tanabe KK. The clinical management of cholangiocarcinoma in the United States and Europe: a comprehensive and evidence-based comparison of guidelines. Ann Surg Oncol. 2021;28(5):2660-2674. doi pubmed
6. Mavros MN, Economopoulos KP, Alexiou VG, Pawlik TM. Treatment and prognosis for patients with intrahepatic cholangiocarcinoma: systematic review and meta-analysis. JAMA Surg. 2014;149(6):565-574. doi pubmed
7. Mazzaferro V, Gorgen A, Roayaie S, Droz Dit Busset M, Sapisochin G. Liver resection and transplantation for intrahepatic cholangiocarcinoma. J Hepatol. 2020;72(2):364-377. doi pubmed
8. Zhang XF, Beal EW, Bagante F, Chakedis J, Weiss M, Popescu I, Marques HP, et al. Early versus late recurrence of intrahepatic cholangiocarcinoma after resection with curative intent. Br J Surg. 2018;105(7):848-856. doi pubmed
9. Zhang XF, Xue F, He J, Alexandrescu S, Marques HP, Aldrighetti L, Maithel SK, et al. Proposed modification of the eighth edition of the AJCC staging system for intrahepatic cholangiocarcinoma. HPB (Oxford). 2021;23(9):1456-1466. doi pubmed
10. Zhang XF, Xue F, Dong DH, Weiss M, Popescu I, Marques HP, Aldrighetti L, et al. Number and station of lymph node metastasis after curative-intent resection of intrahepatic cholangiocarcinoma impact prognosis. Ann Surg. 2021;274(6):e1187-e1195. doi pubmed
11. Zhang XF, Chakedis J, Bagante F, Chen Q, Beal EW, Lv Y, Weiss M, et al. Trends in use of lymphadenectomy in surgery with curative intent for intrahepatic cholangiocarcinoma. Br J Surg. 2018;105(7):857-866. doi pubmed
12. Wei T, Zhang XF, He J, Popescu I, Marques HP, Aldrighetti L, Maithel SK, et al. Prognostic impact of perineural invasion in intrahepatic cholangiocarcinoma: multicentre study. Br J Surg. 2022;109(7):610-616. doi pubmed
13. Huang XT, Huang CS, Li JH, Cai JP, Chen W, Yin XY. Prognostic significance of neutrophil/prealbumin ratio for intrahepatic cholangiocarcinoma undergoing curative resection. HPB (Oxford). 2018;20(12):1215-1222. doi pubmed
14. Hyder O, Hatzaras I, Sotiropoulos GC, Paul A, Alexandrescu S, Marques H, Pulitano C, et al. Recurrence after operative management of intrahepatic cholangiocarcinoma. Surgery. 2013;153(6):811-818. doi pubmed pmc
15. Hu LS, Weiss M, Popescu I, Marques HP, Aldrighetti L, Maithel SK, Pulitano C, et al. Impact of microvascular invasion on clinical outcomes after curative-intent resection for intrahepatic cholangiocarcinoma. J Surg Oncol. 2019;119(1):21-29. doi pubmed
16. Cheng Z, Lei Z, Jin X, Zhang Q, Si A, Yang P, Zhou J, et al. Postoperative adjuvant transarterial chemoembolization for intrahepatic cholangiocarcinoma patients with microvascular invasion: a propensity score analysis. J Gastrointest Oncol. 2021;12(2):819-830. doi pubmed pmc
17. Tang Z, Liu WR, Zhou PY, Ding ZB, Jiang XF, Wang H, Tian MX, et al. Prognostic value and predication model of microvascular invasion in patients with intrahepatic cholangiocarcinoma. J Cancer. 2019;10(22):5575-5584. doi pubmed pmc
18. Lee W, Jeong CY, Jang JY, Roh YH, Kim KW, Kang SH, Yoon MH, et al. Clinical implication of tumor site in terms of node metastasis for intrahepatic cholangiocarcinoma. Eur J Surg Oncol. 2020;46(5):832-838. doi pubmed
19. Li M, Zhou X, Wang W, Ji B, Shao Y, Du Q, Yao J, et al. Selecting an appropriate experimental animal model for cholangiocarcinoma research. J Clin Transl Hepatol. 2022;10(4):700-710. doi pubmed pmc
20. Xu H, Miao X, Chai C, Tang H, Hu J, Zhao Z, Luo W, et al. Establishment and characterization of a new Chinese hepatocellular carcinoma cell line, Hep-X1. Hum Cell. 2023;36(1):434-445. doi pubmed
21. Miao X, Hu J, Chai C, Tang H, Zhao Z, Luo W, Zhou W, et al. Establishment and characterization of a new intrahepatic cholangiocarcinoma cell line derived from a Chinese patient. Cancer Cell Int. 2022;22(1):418. doi pubmed pmc
22. Xu H, Luo W, Zhao Z, Miao X, Chai C, Hu J, Tang H, et al. Establishment and characterization of a new intrahepatic cholangiocarcinoma cell line, ICC-X3. Hum Cell. 2023;36(2):854-865. doi pubmed
23. Fostea RM, Fontana E, Torga G, Arkenau HT. Recent progress in the systemic treatment of advanced/metastatic cholangiocarcinoma. Cancers (Basel). 2020;12(9):2599. doi pubmed pmc
24. Liao W, Feng Q, Liu H, Du J, Chen X, Zeng Y. Circular RNAs in cholangiocarcinoma. Cancer Lett. 2023;553:215980. doi pubmed

25. Mayr C, Kiesslich T, Modest DP, Stintzing S, Ocker M, Neureiter D. Chemoresistance and resistance to targeted therapies in biliary tract cancer: what have we learned? Expert Opin Investig Drugs. 2022;31(2):221-233. doi pubmed
26. Dagogo-Jack I, Shaw AT. Tumour heterogeneity and resistance to cancer therapies. Nat Rev Clin Oncol. 2018;15(2):81-94. doi pubmed
27. Broutier L, Mastrogiovanni G, Verstegen MM, Francies HE, Gavarro LM, Bradshaw CR, Allen GE, et al. Human primary liver cancer-derived organoid cultures for disease modeling and drug screening. Nat Med. 2017;23(12):1424-1435. doi pubmed pmc
28. Kusaka Y, Tokiwa T, Sato J. Establishment and characterization of a cell line from a human cholangiocellular carcinoma. Res Exp Med (Berl). 1988;188(5):367-375. doi pubmed
29. Enjoji M, Sakai H, Nawata H, Kajiyama K, Tsuneyoshi M. Sarcomatous and adenocarcinoma cell lines from the same nodule of cholangiocarcinoma. In Vitro Cell Dev Biol Anim. 1997;33(9):681-683. doi pubmed
30. Shultz LD, Lyons BL, Burzenski LM, Gott B, Chen X, Chaleff S, Kotb M, et al. Human lymphoid and myeloid cell development in NOD/LtSz-scid IL2R gamma null mice engrafted with mobilized human hemopoietic stem cells. J Immunol. 2005;174(10):6477-6489. doi pubmed
31. Shultz LD, Goodwin N, Ishikawa F, Hosur V, Lyons BL, Greiner DL. Human cancer growth and therapy in immunodeficient mouse models. Cold Spring Harb Protoc. 2014;2014(7):694-708. doi pubmed pmc